# Super-resolution imaging of dielectric objects using a slab of left-handed material

Lei Zhao and Tie Jun Cui[a)]
*Center for Computational Electromagnetics, Southeast University, Nanjing 210096, People's Republic of China; State Key Laboratory of Millimeter Waves, Southeast University, Nanjing 210096, People's Republic of China; and Department of Radio Engineering, Southeast University, Nanjing 210096, People's Republic of China*

(Received 1 May 2006; accepted 12 August 2006; published online 2 October 2006)

The Born iterative method has been presented to study two-dimensional inverse scattering problems for dielectric objects with the aid of left-handed material (LHM). Super-resolution imaging can be achieved since the LHM slab could amplify evanescent waves emitted from transmitters, which are interacted with the dielectric objects and then captured by receivers. The evanescent waves contain high-frequency spectra of dielectric objects, leading to significant improvement of resolution in imaging. Simulation results are presented to verify the super-resolution imaging. © *2006 American Institute of Physics*. [DOI: 10.1063/1.2358297]

Electromagnetic inverse scattering methods for reconstruction of dielectric objects from near-field measurements have found wide applications, such as in nondestructive testing, medical imaging, remote sensing, etc.[1–6] As the mathematical relationship between the scattered-field data and the unknown object is nonlinear, it is difficult to solve inverse scattering problems. The Born approximation[6] is a simple and efficient linearized method, which has been widely used to solve free-space and half-space problems when the dielectric objects are weak scatterers.[4–6]

It is important to investigate the resolution achievable in the reconstruction of dielectric objects. As we know, the resolution of imaging using far-field data is 0.5 wavelength according to the Rayleigh criterion,[7] such as in computed tomography (CT) and x-ray tomography. Such a limitation is due to the lack of evanescent waves in the imaging. To overcome the limitation, near-field imaging methods can be applied to capture the evanescent field measurements. Since evanescent waves extract the high-frequency information of objects, a super-resolution may be achieved in object imaging.

In this letter, we will study the super-resolution imaging of dielectric objects using a slab of left-handed material (LHM). To obtain accurate reconstruction results, the Born iterative method (BIM) has been applied. Since the concept of LHM was proposed by Veselago in 1968,[8] intensive studies have been conducted in both theory and experiments.[9–13] With the negative permittivity and negative permeability simultaneously, LHM has been shown to possess a lot of exotic properties such as negative refraction, reversed Doppler shift, and reversed Cerenkov radiation. One of the most attractive features of LHM is the amplification of evanescent waves.[10] Using such a feature, a slightly lossy LHM slab can be made as a superlens.[10–13] In this letter, we make use of the superlens in inverse scattering problems to realize super-resolution images. We show that the image quality using the LHM slab is much better than that from near-field imaging.

We begin with the inverse scattering theory for dielectric objects when a LHM superlens exists. The problem to be considered is shown in Fig. 1. We use multiple transmitters and multiple receivers to collect the scattered data. The transmitters are located at $(x_t,-d_2)$, where $x_t$ is changeable. The receivers are located at $(x_r,z_r)$. If $z_r<-d_2+d_1$, the receivers capture the backward scattered information. If $z_r>z_{\max}$, the receivers capture the forward scattered information. For a transmitter located at $(x_t,z_t)$ where $z_t=-d_2$, the electric field in region 2 is written as

$$E_y^{\mathrm{inc}}(\mathbf{r},\mathbf{r}_t)=i\eta_0 I_t g_t^+(\mathbf{r},\mathbf{r}_t), \tag{1}$$

where $g_t^+$ is Green's function

$$g_t^+(\mathbf{r},\mathbf{r}_t)=\frac{i}{4\pi}\int_{-\infty}^{+\infty} dk_x \frac{1}{k_{0z}} T e^{ik_{0z}(z+d_2)} e^{ik_x(x-x_t)}, \tag{2}$$

in which $k_{0z}=\sqrt{k_0^2-k_x^2}$. Equation (1) is just the incident electric field interacting with the dielectric objects. Under the excitation of such an incident field, there will be electric fields $E_y(\mathbf{r},\mathbf{r}_t)$ induced inside the dielectric objects. From the electromagnetic (EM) theory, we can easily obtain the scattered electric fields due to $E_y(\mathbf{r},\mathbf{r}_t)$:

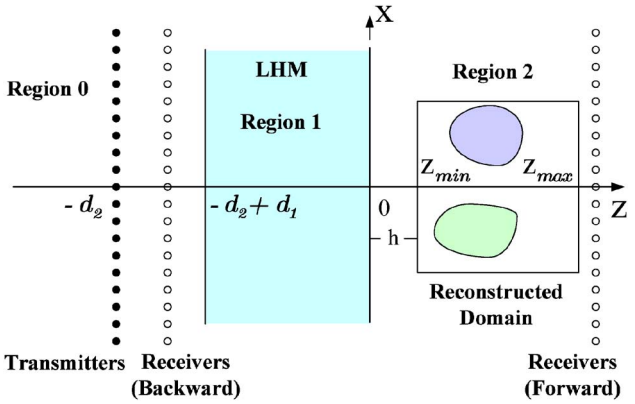


FIG. 1. (Color online) General problem consisting of multiple transmitters, multiple receivers, a LHM slab, and dielectric objects.

[a)]Electronic mail: tjcui@seu.edu.cn

 

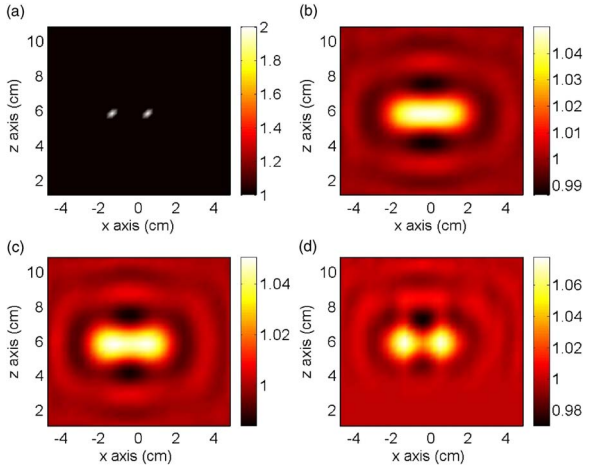


FIG. 2. (Color online) Original and reconstructed profiles for two pointlike objects. (a) Original profile. (b) Reconstructed profile without the LHM slab (near measurements). (c) Reconstructed profile without the LHM slab (very near measurements). (d) Reconstructed profile with the LHM slab (near measurements).

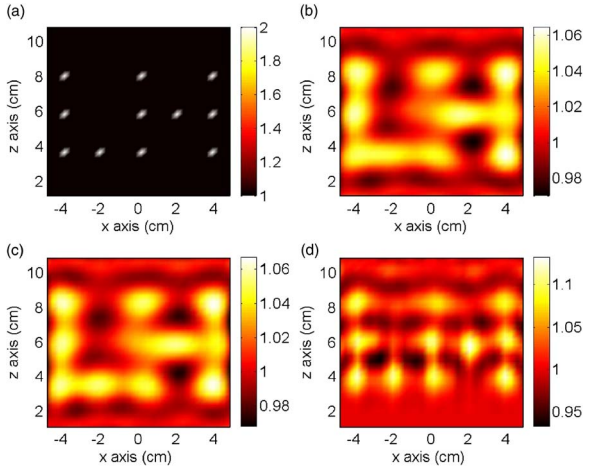


FIG. 3. (Color online) Original and reconstructed profiles for "LH-shaped" pointlike objects. (a) Original profile. (b) Reconstructed profile without the LHM slab (near measurements). (c) Reconstructed profile without the LHM slab (very near measurements). (d) Reconstructed profile with the LHM slab (near measurements).

$$\begin{pmatrix} E_b^{\mathrm{sca}} \\ E_f^{\mathrm{sca}} \end{pmatrix}(\mathbf{r}_r,\mathbf{r}_t) = k_0^2 \int_D d\mathbf{r} \begin{pmatrix} g_t^- \\ g_r \end{pmatrix}(\mathbf{r}_r,\mathbf{r}) E_y(\mathbf{r},\mathbf{r}_t) O(\mathbf{r}), \tag{3}$$

in which $E_b^{\mathrm{sca}}$ and $E_f^{\mathrm{sca}}$ denote the scattered electric fields when the receivers are located backward and forward to the reconstructed objects, respectively (see Fig. 1); $O(\mathbf{r})=\epsilon_r(\mathbf{r})-1$ is the object function, $k_0$ is the wave number in free space, $\epsilon_r(\mathbf{r})$ is the relative permittivity of dielectric objects, and $D$ is the reconstruction domain containing the dielectric objects. Green's functions $g_t^-(\mathbf{r}_r,\mathbf{r})$ and $g_r(\mathbf{r},\mathbf{r}')$ are expressed as

$$g_t^-(\mathbf{r}_r,\mathbf{r}) = \frac{i}{4\pi}\int_{-\infty}^{+\infty} dk_x \frac{1}{k_{0z}} T e^{-ik_{0z}(z_r-z)} e^{ik_x(x_r-x)}, \tag{4}$$

$$g_r(\mathbf{r},\mathbf{r}') = \frac{i}{4} H_0^{(1)}(k_0|\mathbf{r}-\mathbf{r}'|) + \frac{i}{4\pi}\int_{-\infty}^{+\infty} dk_x \frac{1}{k_{0z}} R e^{ik_{0z}(z+z')} e^{ik_x(x-x')}, \tag{5}$$

where $R$ and $T$ are the reflection and transmission coefficients. From the boundary conditions, we have

$$R = \frac{R_{01}+R_{12}e^{i2k_{1z}d}}{1+R_{01}R_{12}e^{i2k_{1z}d}}, \tag{6}$$

$$T = \frac{4e^{-ik_{0z}d}e^{ik_{1z}d}}{(1+P_{01})(1+P_{12})[1+R_{01}R_{12}e^{i2k_{1z}d}]}, \tag{7}$$

in which $d=d_2-d_1$ is the thickness of LHM slab, $k_{iz}=\sqrt{k_i^2-k_y^2}(i=0,1,2)$ is the propagating factor in region $i$, and $R_{01}=(1-P_{01})/(1+P_{01})$ and $R_{12}=(1-P_{12})/(1+P_{12})$ are Fresnel reflection coefficients at slab interfaces with $P_{01}=(\mu_0 k_{1z})/(\mu_1 k_{0z})$ and $P_{12}=(\mu_1 k_{0z})/(\mu_0 k_{1z})$. Hence, Eq. (3) can be generally written as

$$E^{\mathrm{sca}}(\mathbf{r}_r,\mathbf{r}_t) = k_0^2 \int_D d\mathbf{r} g(\mathbf{r}_r,\mathbf{r}) E_y(\mathbf{r},\mathbf{r}_t) O(\mathbf{r}). \tag{8}$$

The above equation is indeed a nonlinear integral equation for the object function $O(\mathbf{r})$, since $E_y(\mathbf{r},\mathbf{r}_t)$ is also related to $O(\mathbf{r})$ by the following integral equation:

$$E_y(\mathbf{r},\mathbf{r}_t) - k_0^2 \int_D d\mathbf{r}' g_r(\mathbf{r},\mathbf{r}') O(\mathbf{r}') E_y(\mathbf{r}',\mathbf{r}_t) = E_y^{\mathrm{inc}}(\mathbf{r},\mathbf{r}_t). \tag{9}$$

Obviously, the Born approximation of the internal electric field $E_y(\mathbf{r},\mathbf{r}_t)$ will result in a linearized inverse scattering equation

$$E^{\mathrm{sca}}(\mathbf{r}_r,\mathbf{r}_t) = k_0^2 \int_D d\mathbf{r} g(\mathbf{r}_r,\mathbf{r}) E_y^{\mathrm{inc}}(\mathbf{r},\mathbf{r}_t) O(\mathbf{r}). \tag{10}$$

The above equation can be easily solved using the Tikhonov regularization technique.[14] Using the reconstructed object function, the total electric field $E_y(x,y)$ can be computed by a fast forward solver. Then the nonlinear integral equation (8) becomes a linear one, from which the object function can be updated. Repeating the above procedure yields the Born iterative method.[2]

To demonstrate the feasibility of inversion involving the LHM slab, we have numerically simulated the reconstruction of $O(\mathbf{r})$ for a collection of pointlike objects. Here the scattered data are simulated by solving the forward problem using an accurate method[12] by adding 10% white noise.

In the following numerical examples, the LHM slab is described by the Lorentz medium model,[9]

$$\epsilon_{r1} = 1 - \frac{\omega_{ep}^2 - \omega_{eo}^2}{\omega^2 - \omega_{eo}^2 + i\gamma\omega}, \tag{11}$$

$$\mu_{r1} = 1 - \frac{\omega_{mp}^2 - \omega_{mo}^2}{\omega^2 - \omega_{mo}^2 + i\gamma\omega}, \tag{12}$$

where $\omega_{eo}$ and $\omega_{mo}$ are electric and magnetic resonant frequencies, $\omega_{ep}$ and $\omega_{mp}$ are electric and magnetic plasma frequencies, and $\gamma$ is the loss factor. In our numerical experi-

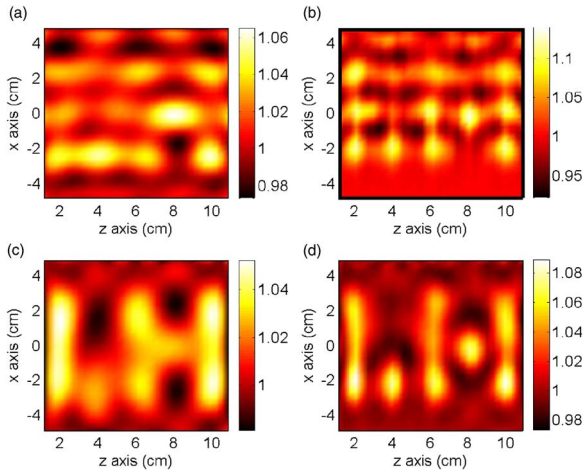


FIG. 4. (Color online) Reconstructed profiles for "LH-shaped" pointlike objects using either backward or forward receivers. (a) Without the LHM slab (very near measurements) using only backward receivers. (b) With the LHM slab (near measurements) using only backward receivers. (c) Without the LHM slab (very near measurements) using only forward receivers. (d) With the LHM slab (near measurements) using only forward receivers.

ments, we choose $f_{eo}=f_{mo}=1.26$ GHz, $f_{ep}=f_{mp}=7.245$ GHz, and $\gamma=1.0$ MHz, and the working frequency is 5.2 GHz. The LHM slab is resided at $d_1=5$ cm and $d_2=15$ cm, as shown in Fig. 1. The reconstruction domain is chosen as $10\times10$ cm$^2$ region, and $h=1$ cm. Such a reconstruction domain contains $32\times32=1024$ pixels. We use 35 transmitters, 35 backward receivers, and 35 forward receivers, which are placed on the measurement lines $z=-15$ cm, $-14$ cm, 11.1 cm, respectively, to collect scattered data over a range of 50 cm. We refer such measurements as "near measurements."

To view the effect of LHM slab on the imaging resolution, we compare the reconstruction results with and without the LHM slab. The inversion results for pointlike dielectric objects after ten BIM iterations are plotted in Figs. 2 and 3, where each pointlike object has a size of $0.3125\times0.3125$ cm$^2$ and a relative permittivity of 2. In above figures, (a) represents the original object profiles; (b) gives the reconstructed profiles without the LHM slab; (c) demonstrates the reconstructed profiles without the LHM slab when the transmitters and receivers are placed much nearer to the dielectric objects ($z_t=-1$ cm, $z_{r1}=0$, $z_{r2}=11.1$ cm), which is referred as "very near measurements;" and (d) shows the reconstructed profiles with the LHM slab.

In Fig. 2, we consider two pointlike objects whose distance is 1.56 cm (0.27 wavelength). When the LHM slab does not exist, the BIM reconstruction result is illustrated in Fig. 2(b). Clearly, the two objects cannot be detected at all. Even when the transmitters and receivers are moved very closer to the objects ($z_t=-1$ cm, $z_{r1}=0$, $z_{r2}=11.1$ cm), the near-field inversion is also unsatisfactory for pointlike objects, as shown in Fig. 2(c). Using the LHM slab, however, a super-resolution image is achieved where the two objects are well separated, as demonstrated in Fig. 2(d).

Figure 3 gives a more complicated example where "LH-shaped" 11 pointlike objects are contained in the reconstruction domain. Again, imaging results without and with the LHM slab are given. Comparing these results, we observe that the LHM superlens can obviously enhance the imaging resolution. The image quality using the superlens [see Fig. 3(d)] is much better than that from near-field measurements [see Figs. 3(b) and 3(c)].

The main physical reason for super-resolution is because the evanescent waves emitted from transmitters are amplified by the superlens, which are then interacted with the dielectric objects. The information carrying the evanescent components of objects are amplified again to be captured by receivers. The richness of evanescent information leads to the super-resolution imaging.

To demonstrate the above physical reason further, we consider two more reconstruction results. In earlier examples, both forward and backward receivers are used to obtain the forward and backward scattering information. If we only use the 35 backward receivers, the imaging results without and with the LHM slab are illustrated in Figs. 4(a) and 4(b), where very near measurements have been used in Fig. 4(a) for a fair comparison ($z_t=-1$ cm, $z_{r1}=0$). Obviously, the use of LHM superlens improves the image quality significantly in this case. Comparing Figs. 3(c) and 4(a), the lack of forward receivers has more impact on imaging when the superlens does not exist since the forward receivers have the same importance as the backward ones in capture of near-field information. When the superlens exists, however, the backward receivers are much more important because both evanescent waves from transmitters and scatterers are amplified and used in imaging. This can be clearly seen in Fig. 4(b), which has a similar quality to Fig. 3(d). If we only use forward receivers for reconstruction, the imaging is not so good since the evanescent waves from scatterers cannot be amplified by the superlens, as illustrated in Figs. 4(c) and 4(d).

In conclusion, we propose an inversion algorithm to reconstruct dielectric objects using a LHM superlens. It has been shown that the superlens helps to capture more evanescent waves in inverse scattering, resulting in super-resolution images. Numerical experiments validate the above conclusions.

This work was supported in part by the National Science Foundation of China for Distinguished Young Scholars under Grant No. 60225001, in part by the National Basic Research Program (973) of China under Grant No. 2004CB719800, and in part by the National Doctoral Foundation of China under Grant No. 20040286010.

[1] A. J. Devaney, Opt. Lett. **6**, 374 (1981).
[2] W. C. Chew and Y. M. Wang, IEEE Trans. Med. Imaging **9**, 218 (1990).
[3] F. C. Chen and W. C. Chew, Appl. Phys. Lett. **72**, 3080 (1998).
[4] M. Born and E. Wolf, *Principles of Optics* (Pergamon, New York, 1980), Vol. 4, p. 131.
[5] T. B. Hansen and P. M. Johansen, IEEE Trans. Geosci. Remote Sens. **38**, 496 (2000).
[6] T. J. Cui and W. C. Chew, IEEE Trans. Antennas Propag. **50**, 42 (2002).
[7] T. J. Cui, W. C. Chew, X. X. Yin, and W. Hong, IEEE Trans. Antennas Propag. **52**, 1398 (2004).
[8] V. G. Veselago, Sov. Phys. Usp. **10**, 509 (1968).
[9] R. A. Shelby, D. R. Smith, and S. Schultz, Science **292**, 77 (2001).
[10] J. B. Pendry, Phys. Rev. Lett. **85**, 3966 (2000).
[11] T. J. Cui, Z. C. Hao, X. X. Yin, W. Hong, and J. A. Kong, Phys. Lett. A **323**, 484 (2004).
[12] L. Zhao and T. J. Cui, Phys. Rev. E **72**, 061911 (2005).
[13] N. Fang, H. Lee, C. Sun, and X. Zhang, Science **308**, 534 (2005).
[14] S. Twomey, *Introduction to the Mathematics of Inversion in Remote Sensing and Indirect Measurements*, (Elsevier, New York, 1977).